RSC Sustainability

ROYAL SOCIETY OF CHEMISTRY

PAPER

View Article Online
View Journal | View Issue

Cite this: *RSC Sustainability*, 2023, **1**, 2081

ZIF-8 derived ZnO: a facile catalyst for ammonium perchlorate thermal decomposition†

Gladiya Mani, [a] Aswathy V. Kumar[a] and Suresh Mathew *[ab]

The growing interest in sustainable technology advancements necessitates the development of green and environmentally benign facile catalysts for rocket propellants, which eliminates the use of toxic and/or hazardous reagents and encourages the efficient use of base metals. Here, ZIF-8 was employed as a sacrificial template for the synthesis of porous, low-cost, simple and eco-friendly ZnO *via* simple calcination for the thermal decomposition studies of ammonium perchlorate (AP). Structural analyses reveal that the complete conversion of ZIF-8 to ZnO occurs only at high temperatures. Prolonged calcination results in the lowering of the band gap, the availability of more polar planes and the presence of oxygen defects on the ZnO surface, which facilitate the faster decomposition of perchloric acid and ammonia intermediates of AP decomposition. In the presence of 1 wt% ZnO calcined at 500 °C (Z500), the two-stage decomposition pattern shows an amalgamation tendency with a significant reduction in decomposition temperature (90 °C), followed by a significant drop in the activation energy from 149 kJ mol^{-1} to 130 kJ mol^{-1} in the presence of Z500. Later, TG-MS analysis shows the catalyzed AP decomposition *via* the evolution patterns of decomposition products NO, NO_2, N_2O, Cl, HCl, NH_2, O_2 and Cl_2. Hence, ZIF-8-derived ZnO is a facile catalyst as it effectively catalyzes the AP thermal decomposition with a minimal catalytic content and eco-friendly synthesis procedure.

Received 27th July 2023
Accepted 2nd October 2023

DOI: 10.1039/d3su00256j

rsc.li/rscsus

Sustainability spotlight

Conventionally used propellant catalysts are expensive and polluting, involving hazardous reagents and toxic chemicals for their complex synthesis. Recently, MOF-based catalysts have been employed in larger quantities to achieve excellent results, which in turn will adversely affect the propellant's energetics. Therefore, zeolitic imidazole framework (ZIF)-8 derived porous, facile, cheap, and eco-friendly zinc oxide was synthesized as an efficient catalyst with minimal usage for ammonium perchlorate (AP) decomposition in propellants using a green solvent (water), in contrast to traditional methanol-based synthesis. Moreover, the exceptional efficiency of the synthesized catalyst along with its biocompatible features reduces toxicity concerns and encourages its use in solid propellants. ZIF-based catalysts will also help bring sustainability to propellant research without compromising their energetics. This work is in line with the UN's Sustainable Development Goals 12 and 17, which demand the sustainable consumption of resources and production for the implementation of sustainable development.

Introduction

Rockets, missiles, and propellants constitute an integral part of military arsenals, space missions, and satellite launching.[1–3] A high-performance solid propellant, the key energy source of rocket motors, is a prerequisite for long-range launching.[3,4] Composite solid propellants (CSPs) are mainly composed of oxidizers, binders, and some functional additives.[5] Ammonium perchlorate (AP), the most commonly used oxidizer, comprises around 60–90% of the total content of CSPs and is known for its high oxygen level, high thermal stability, large combustion gas production per unit content, and great oxidation performance.[4,6] Owing to the aforementioned properties, AP is regarded as an irreplaceable oxidizer. Being the major component, the thermal behaviour of AP directly influences the propellant performance and is highly sensitive to the presence of additives.[6–8] And, this has laid the path for the development of various catalytic systems, including metal oxides, 1-D and 2-D carbon materials, and many others,[9–11] to improve the effectiveness of catalytic AP thermolysis.

Efforts to integrate sustainability into propellant research have come up with the idea of developing green catalysts without sacrificing the energetics of propellants. Compared to conventional expensive catalysts, base metal oxide-mediated AP thermolysis with minimal catalyst content is receiving ample attention as a green alternative. This prevents extra propellant dead weight, hazardous waste release and their accumulation in

[a]*School of Chemical Sciences, Mahatma Gandhi University, Kottayam 686560, Kerala, India. E-mail: sureshmathewmgu@gmail.com*

[b]*Advanced Molecular Materials Research Centre, Mahatma Gandhi University, Kottayam 686560, Kerala, India*

† Electronic supplementary information (ESI) available. See DOI: https://doi.org/10.1039/d3su00256j

space. Zinc oxide (ZnO), an n-type semiconductor, has been well-researched as a catalyst for AP decomposition studies due to its easy availability, low cost, facile synthesis, and eco-friendliness.[12] Mostly, zinc oxide was used in the form of pure ZnO,[13] binary composites,[12] bimetallic oxides,[6] and hierarchical nanostructures.[14]

Recently, metal–organic frameworks (MOFs) have fascinated the research community as a sacrificial template to fabricate transition metal oxides by simple calcination for versatile applications. MOFs as a metal oxide template offer great stability, a significant surface area, and a highly ordered crystalline structure, which aid in the creation of tunable nanomaterials, in contrast to conventional metal oxide precursors.[15] The calcination of MOFs in air results in the decomposition of ligands to oxides of carbon and nitrogen, leaving the free metal atoms to react with oxygen to form porous metal oxides.[16] Guo *et al.* explored the effect of HKUST-1-derived micro-structured CuO in AP thermal decomposition studies. The results show that by adding 10 wt% CuO, both decomposition temperature and E_a values were significantly reduced.[17] Similarly, CuO-MOF derived $Cu/Cu_2O/C$ synthesized by Yan *et al.* was found to be a promising catalyst for AP thermolysis due to its abundant pore structure and good synergy between Cu nanoparticles and the carbon present.[18] Likewise, flexible iron-based MIL-88B and Cu(II)–MOFs were also employed as catalysts for AP pyrolysis studies. The MIL-88 B-based catalyst resulted in a 66% increase in decomposition enthalpy and around a 25% decrease in E_a. Meanwhile the latter exhibited outstanding catalytic efficiency in both AP and RDX decomposition.[19,20] Similarly, metal complexes[21] (like Prussian blue) are also being well explored as positive catalysts for AP decomposition due to their dispersed active sites, simple synthesis, efficient catalytic nature and tunability in ligands according to the applications. These metal complexes decompose at very low temperatures (ahead of AP) leaving metal oxides in the system that will further catalyze AP thermolysis by increased availability of active oxygen and faster oxidation of N to NO, NO_2 and N_2O.[22,23] Zeolitic imidazole frameworks (ZIFs) – a subfamily of MOFs, have recently been in the limelight due to their excellent properties. ZIF-8 (zinc-based MOF) calcination is regarded as the simplest technique to yield crystalline, porous ZnO, which offers more active sites and faster absorption of reaction molecules onto the surface. Recently, ZIF-67-based catalysts have been widely employed for the thermal decomposition studies of AP. Interestingly, the thus formed cobalt oxide shows excellent catalytic activity by significantly reducing HTD temperature as well as the apparent activation energy of AP decomposition.[11,24,25] Even though MOF-based catalysts are quite efficient, they have been used in larger amounts to get higher values of decomposition temperature. Through his work, we have tried to develop a ZIF-based highly efficient catalyst, which can achieve good results with minimal catalytic content.

Compared to traditional, expensive, and toxic metal oxide catalysts with complex synthesis procedures, the development of green and facile catalysts which are easily available, economical, and prepared by environmentally benign techniques (by replacing hazardous reagents) has become the need of the hour. In this study, ZIF-8 was employed as the sacrificial template to yield porous ZnO nanoparticles *via* simple calcination in air. The synthesis of ZIF-8 was carried out in water as a medium with minimal reagent requirement (Scheme 1), followed by calcination. The effect of calcination temperatures on ZnO towards catalyzing AP thermolysis was explored in detail. Thermal analyses suggest that ZnO synthesized at 500 °C exhibits maximum catalytic activity by reducing both the activation energy and the HTD temperature of AP thermal decomposition. This research provides some new insights into the synthesis of sustainable, facile, low-cost, eco-friendly, and efficient catalysts for AP thermal decomposition studies with minimal catalytic content. This study extends an effort to understand the role of calcination temperatures in determining the catalytic efficiency of ZIF-8-derived porous ZnO towards AP thermolysis.

Experimental

Materials and methods

The following chemicals of analytical grade were purchased and were used as received. Zinc nitrate hexahydrate (Sigma Aldrich), 2-methylimidazole (HiMedia) and ammonium perchlorate (APEP, ISRO-Aluva, Kerala, India).

Synthesis of ZIF-8 and ZnO

ZIF-8 was synthesized at room temperature in an aqueous system by using $Zn(NO_3)_2 \cdot 6H_2O$ and 2-methylimidazole. About

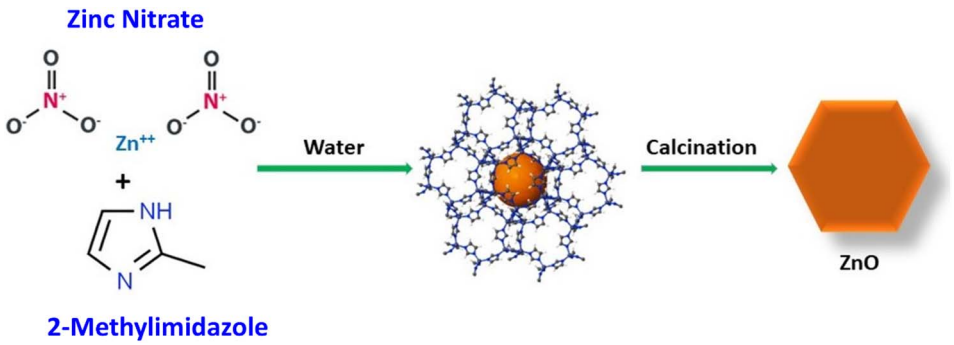

Scheme 1 Schematic illustration of the synthesis of ZnO from ZIF-8.

2.376 g of $Zn(NO_3)_2 \cdot 6H_2O$ was dissolved in 40 mL of deionized water and 1.312 g of 2-methylimidazole was dissolved in 40 mL of deionized water to yield zinc nitrate and 2-methyl imidazole solutions, respectively. To synthesize ZIF-8 crystals, the zinc nitrate aqueous solution was added into the 2-methylimidazole aqueous solution under stirring. The mixture was then stirred at room temperature for 4 h for the crystallization of ZIF-8. After the reaction, ZIF-8 powders were collected by repeated centrifugation and washed with methanol and deionized water, followed by drying at 70 °C overnight. Porous ZnO was prepared by the calcination of ZIF-8 in the air at 300 °C, 500 °C, and 750 °C for 5 h. The obtained ZnO was then used for further analyses. A schematic representation of the synthesis procedure is given in Scheme 1.

Materials characterization

Powder XRD of the synthesized samples was done using a Rigaku Miniflex benchtop X-ray diffractometer with monochromatized Cu-Kα ($\lambda = 1.5425$ Å) incident radiation with a scan range of 2θ 5–80°. The FT-IR spectra of samples were recorded on a PerkinElmer 400 spectrometer in the wavelength range 400–4000 cm^{-1}. SEM images with EDAX analysis were recorded using a Carl Zeiss Supra 55 model field emission scanning electron microscope coupled with Bruker XFlash 7 EDS instrument to evaluate the morphology and elemental composition of the synthesized sample. High-resolution TEM images were taken using a JEOL JEM-2100 microscope at an accelerating voltage of 200 kV. Using a Quantachrome Nova Touch Ix4 Analyzer, the Brunauer–Emmett–Teller (BET) surface area and Barrett–Joyner–Halenda (BJH) pore structure calculations were done. The UV-vis diffusion reflectance spectra were recorded on a Shimadzu UV 2450 UV-vis spectrophotometer to calculate the bandgaps of the synthesized samples. For carrying out the thermal analyses, catalysts were mixed with AP in a mass ratio of 1 : 99 using a mortar and pestle. TG analysis was done in a helium atmosphere with a sample mass of 6.4 mg, a 75 mL min^{-1} purging rate and a heating rate of 3.5 °C min^{-1}. Thermograms were recorded on a PerkinElmer TGA 8000. DSC analysis was done using a TA instrument SDT Q-600 in an argon atmosphere at a heating rate of 5 °C min^{-1}. TG-MS analysis was performed on a PerkinElmer TGA 8000 coupled with a PerkinElmer Clarus 680 Gas Chromatogram-PerkinElmer Clarus SQ 8T mass spectrometer at a heating rate of 3.5 °C min^{-1}. XPS spectra were recorded using a ULVAC-PHI 5000 VersaProbe II equipped with a micro-focused (100 μm, 15 kV) monochromatic Al-Kα X-ray source ($h\nu$ = 1486.6 eV). The binding energy was referenced to the C 1s peak at 284.8 eV.

Results and discussion

XRD analysis

The crystal structures of the synthesized ZIF-8 and ZIF-8-derived ZnO samples were analyzed using XRD. A comparison of the X-ray diffraction pattern of the synthesized ZIF-8 with simulated data is given in Fig. S1.† According to Fig. S1,† the sharp diffraction peaks of prepared ZIF-8 are in good agreement with

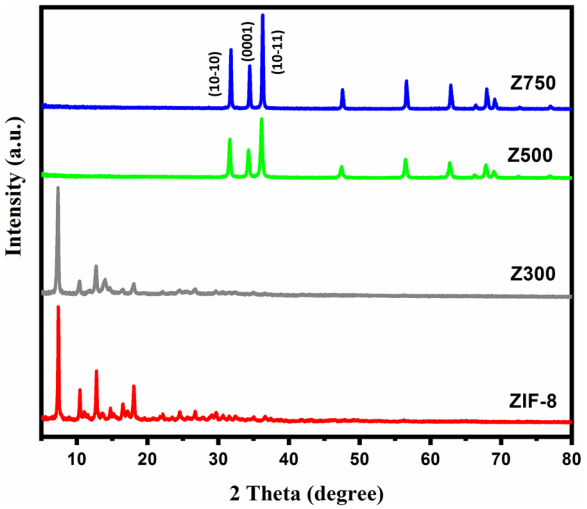

Fig. 1 XRD patterns of ZIF-8, Z300, Z500 and Z750.

the simulated data (CCDC 602542)[26] and previous reports,[27] inferring good crystallinity and phase purity of the synthesized sample. Similarly, the XRD patterns of calcined ZnO samples are given in Fig. 1. Here we can see that, for Z300, even after calcining the sample at 300 °C for 5 h, complete conversion of ZIF-8 to ZnO doesn't occur. Instead, diminished peak intensity (except for the intense peak at 7.3°) was observed, which implies that the ZIF-8 structure has started to collapse due to prolonged calcination. As we increased the calcination temperatures from 300 °C to 500° and 750 °C, reflections corresponding to ZIF-8 started to vanish and peaks corresponding to ZnO started to appear. The intense sharp peaks of Z500 and Z750 suggest that complete calcination of ZIF-8 to ZnO occurs only at higher temperatures, leading to the formation of highly crystalline phase pure hexagonal ZnO (JCPDS No. 36-1451).[28] The calculated cell parameters (a = 0.326 nm and c = 0.523 nm) are also compatible with the literature values of the above JCPDS card.[29]

Depending on the crystal faces that are exposed, crystalline materials have distinct characteristics and behaviours. And, the prospective applications of these crystalline structures as intelligent and efficient materials are largely dependent on the exposed crystal faces. Based on the reports, ZnO with exposed (0001) crystal facets was found to be more chemically active than other structures.[13,30,31] Also, consulting the aforementioned JCPDS no, the diffraction intensities of the (10−10) and (10−11) planes are relatively higher than that of the (0001) plane. However, as per the report of Tang *et al.*, a larger intensity ratio of the (0001) polar facet to the (10−10) non-polar plane ($I_{(0001)}/I_{(10-10)}$) implies an increased (0001) facet in the synthesized ZnO.[32] In our case, this intensity ratio follows the trend Z500 > Z750 (*i.e.* for Z500, the $I_{(0001)}/I_{(10-10)}$ value is 0.737 and for Z750 it is 0.706), which means the availability of more polar (0001) planes on the Z500 surface. Therefore, the occurrence of abundant (0001) facets in Z500 will facilitate the faster decomposition of AP and consequently a higher burn rate. Furthermore, the higher catalytic activity of ZnO samples with large polar planes can be attributed to the easiness of polar planes in

generating oxygen vacancies.[33] Hence, the above findings validate the superior catalytic efficacy of Z500 over Z750 towards AP thermolysis.

FTIR analysis

The formation of synthesized ZIF-8 and ZIF-derived ZnO at various calcination temperatures was further analyzed by Fourier transform infrared spectroscopy (FT-IR) analysis. The absorptions corresponding to each functional group present are plotted and given in Fig. 2. The FTIR spectra of ZIF-8 show that there is a sharp peak at 421 cm^{-1} attributed to the presence of Zn–N stretch mode, demonstrating a strong interaction between zinc and nitrogen atoms to form the ZIF coordination structure[34] (Fig. S2†). Peaks at 692 and 757 cm^{-1}, and 994 and 1179 cm^{-1} were attributed to the out-of-plane and in-plane bending of the imidazole ring.[35,36] A strong peak in the region 1300–1450 cm^{-1} indicates the C–N absorption band. Peaks at 1421 and 1309 cm^{-1} belonging to 2-methylimidazol are observed in the FTIR spectra of ZIF-8 and ZnO-300, indicating the presence of organic ligands. In contrast, the 2-methylimidazol peaks vanished in ZnO-500 and ZnO-750, implying that ZIF-8 has been completely decomposed.[37] The stretching vibrations of Zn–O are attributed to the absorption bands at 400–550 cm^{-1} in the spectra of ZnO-500 and ZnO-750, confirming the formation of ZnO.[38] When the temperature reaches 500 °C, all other peaks of ZIF-8 disappear from the spectra indicating the dissociation of the Zn-2-methyl imidazolate coordination structure and formation of ZnO. Similarly, for ZnO-750, the FT-IR spectra show no characteristic peaks of ZIF-8 suggesting the entire disintegration of ZIF-8.

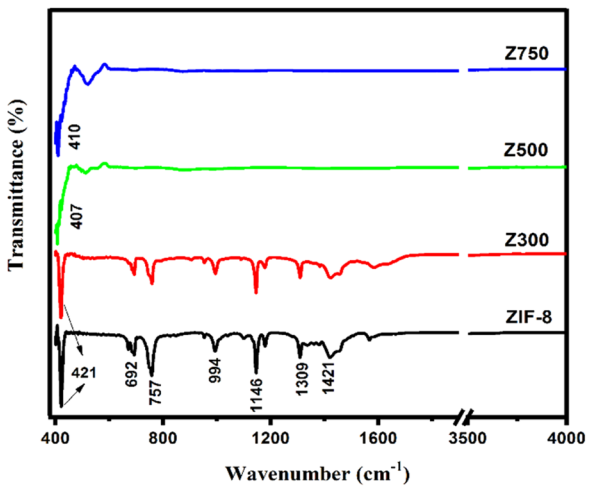

Fig. 2 FTIR spectra of ZIF-8, Z300, Z500, and Z750.

Morphology analysis

The morphology of the material is said to have a telling effect on determining numerous properties and thus its versatile applications. Here, morphology analyses were done using FE-SEM, TEM, and EDS techniques. The FE-SEM analysis of Z500 (Fig. 3a and b) shows that the synthesized ZnO particles are in the nanometer regime, whose size comes under <100 nm. Even though most of the ZnO particles are very small in size (of the

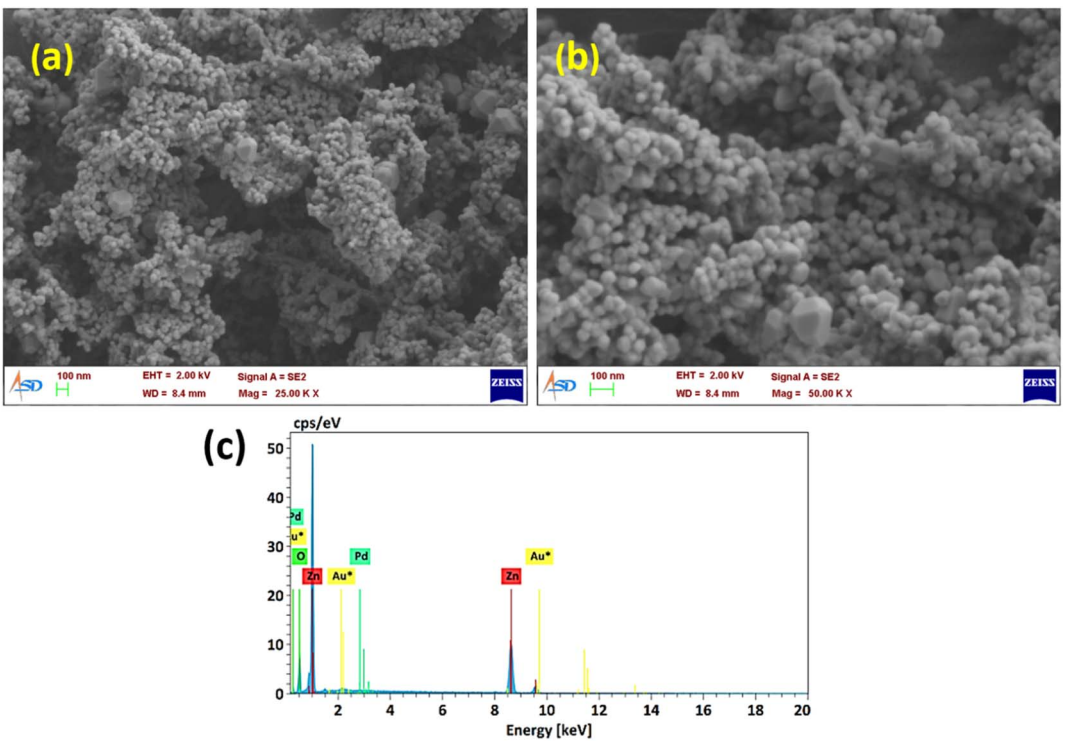

Fig. 3 FE-SEM (a and b) images at different magnifications and (c) EDX analysis of Z500.

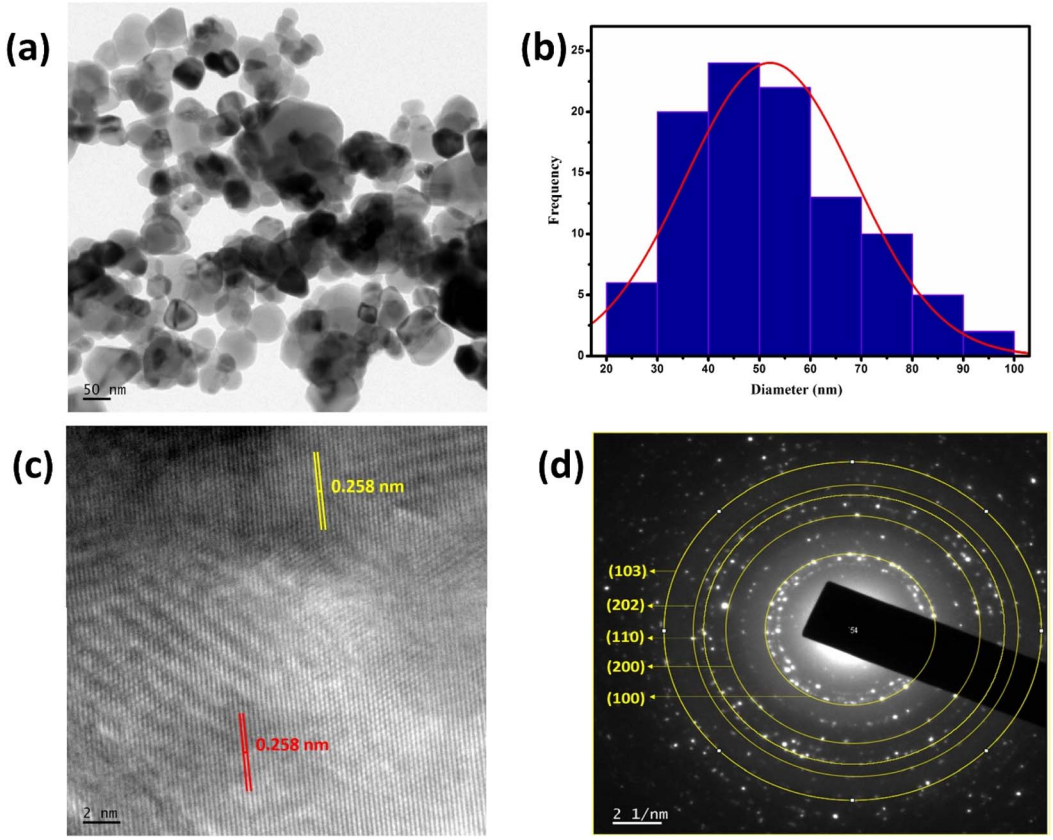

Fig. 4 (a) TEM image, (b) histogram showing the particle size distribution, (c) HR-TEM image and (d) SAED pattern of Z500.

nanometer range as mentioned above), a few of them are large in dimensions, *i.e.*, higher than 100 nm with a polyhedron structure. The EDX analysis (Fig. 3c) shows the elemental composition of the synthesized Z500 sample. The result validates the presence of only Zn and O in the sample and thus its compositional purity.

Furthermore, TEM analysis of the sample was done to understand the structural properties in detail. The transmission electron microscopy images (Fig. 4a) show that all the ZnO particles formed have an irregular morphology with an average size of around 50 nm. Also, there are a few particles with higher dimensions of around 100 nm. These observations were confirmed by the particle size distribution curve shown in Fig. 4b. From the given histogram we observed that the size of the synthesized particles is in the range of 20–100 nm with an average particle size of 52 nm. From the HR-TEM image (Fig. 4c), the *d*-spacing was calculated and was found to be 0.258 nm corresponding to the (002) plane of ZnO,[39] which is congruent with the XRD findings. Hence, HR-TEM analysis also affirms the formation of ZnO by the calcination of ZIF-8 at 500 °C. Similarly, the SAED pattern (Fig. 4d) shows the presence of concentric circles of bright spots, which can be attributed to the polycrystalline nature of synthesized Z500. Also, using the diameters of these circles, *d*–*d*-spacings were calculated to be 0.287 nm, 0.193 nm, 0.162 nm, 0.128 nm, and 0.145 nm, implying the presence of (100), (200), (110), (202), and (103)[39] planes, respectively. These observations again authenticate the formation of wurtzite ZnO.

UV-vis diffuse reflectance spectra

The UV-vis DRS of all the prepared samples were recorded to understand the role of calcination temperatures in tuning their band gaps (E_g). Hence, the E_g values of the synthesized samples were calculated using the Kubelka–Munk equation and the corresponding Tauc-plots are given in Fig. S4.† The band gap values for synthesized ZIF-8, Z300, Z500, and Z750 are 5.21 eV, 5.17 eV, 3.22 eV, and 3.11 eV respectively.

As the annealing temperature increases from 300 °C to 750 °C, the band gap value decreases, which validates the aforementioned claim that MOF-derived materials are highly tunable. Here, we can see that the band gap of Z300 is very close to that of ZIF-8, which again affirms the fact that Z300 has more ZIF-8 traits than ZnO as shown in XRD and FT-IR results. In the case of Z500 and Z750, they have all the characteristics of ZnO, which are evident from their band gap values, which are approximately 3.2 eV. With the low band gaps of Z500 and Z750, it will be easy for the electrons to get excited from the valence band to the conduction band, resulting in the availability of more electron–hole pairs for catalysis. These free charge carriers will be then taken up by the decomposition reaction intermediates (perchloric acid and ammonia) to get reduced and oxidized respectively leading to faster decomposition of AP.

BET analysis

The surface and porous features of the synthesized samples were investigated using the N_2 adsorption–desorption method.

Table 1 Surface and porous parameters of the samples

Sample	BET surface area ($m^2\ g^{-1}$)	Avg. pore radius (nm)	Avg. pore volume ($cm^3\ g^{-1}$)
Z300	494	1	0.3
Z500	9	4	0.02
Z750	5	3	0.01

The Brunauer–Emmett–Teller (BET) surface areas and corresponding isotherms are given in Fig. S5.† The decrease in the specific surface area and pore volume during the annealing process from 494 $m^2\ g^{-1}$ (Z300) to 5.5 $m^2\ g^{-1}$ (Z750) is given in Table 1. For Z300 (Fig. S5a†), the nitrogen sorption isotherm shows a significant uptake in the relatively low-pressure region $P/P_o < 0.1$ followed by a hysteresis loop in the high-pressure range. This sort of isotherm can be identified as the combination of type I and type IV isotherms,[40] implying the coexistence of micropores and mesopores in Z300. In the case of Z500, the isotherm belongs to type IV with an H3 hysteresis loop at high pressure accounting for the mesoporous nature of the synthesized ZnO. As per Table 1, Z750 possess the least surface area and pore volume. The adsorption and desorption branches of Z750 just overlapped without forming any hysteresis loop, implying the non-porous nature of Z750. The pore size distribution curves (Fig. S6†) reveal that the distribution of pores mostly lies in the range of 1–8 nm radii. According to Table 1, Z500 has the maximum pore radius and is mesoporous in nature and responsible for the hysteresis loop in the isotherm at higher pressure. This kind of porous structure will be highly beneficial for catalytic efficiency as it helps in the effectual trapping of decomposition products like perchloric acid and ammonia onto the catalyst surface and faster decomposition of AP on the ZnO surface. From the nitrogen sorption analysis, we could infer that, as the calcination temperature increases, corresponding decreases in the surface area and pore volume were observed. This may possibly be due to the decomposition of ligands and the collapse of the framework due to prolonged heating.

XPS analysis

To understand the chemical state as well as the elemental composition of the prepared samples Z300, Z500 and Z750, XPS analysis was employed. The XPS survey spectra given in Fig. 5, S7 and S8† depict the surface elements present, including Zn, O, C and N in the samples. The strong and broad peak observed at 398.9 eV in the N 1s spectrum of Z300 indicates the presence of ligand nitrogen,[41] confirming the incomplete conversion of ZIF-8 to ZnO, consistent with our XRD and FT-IR findings. As the calcination temperature increases, no such peak was observed in Z500 and Z750, implying the destruction of the ZIF-8 framework at higher temperatures. Also, with increasing calcination temperature, intense O 1s peaks were observed in Z500 and Z750, corresponding to the complete conversion of ZIF-8 to ZnO at higher temperatures. For Z300, a small O 1s peak in the survey spectrum may be attributed to the adsorbed CO_2 and H_2O molecules on the sample surface.[42] With increasing calcination temperature, carbonization or carbon content in the sample also increases (Fig. 5 and S8†). From Fig. 5, the high-resolution spectrum of the C 1s peak can be deconvoluted into two peaks, a major peak at 284.8 eV and another one at

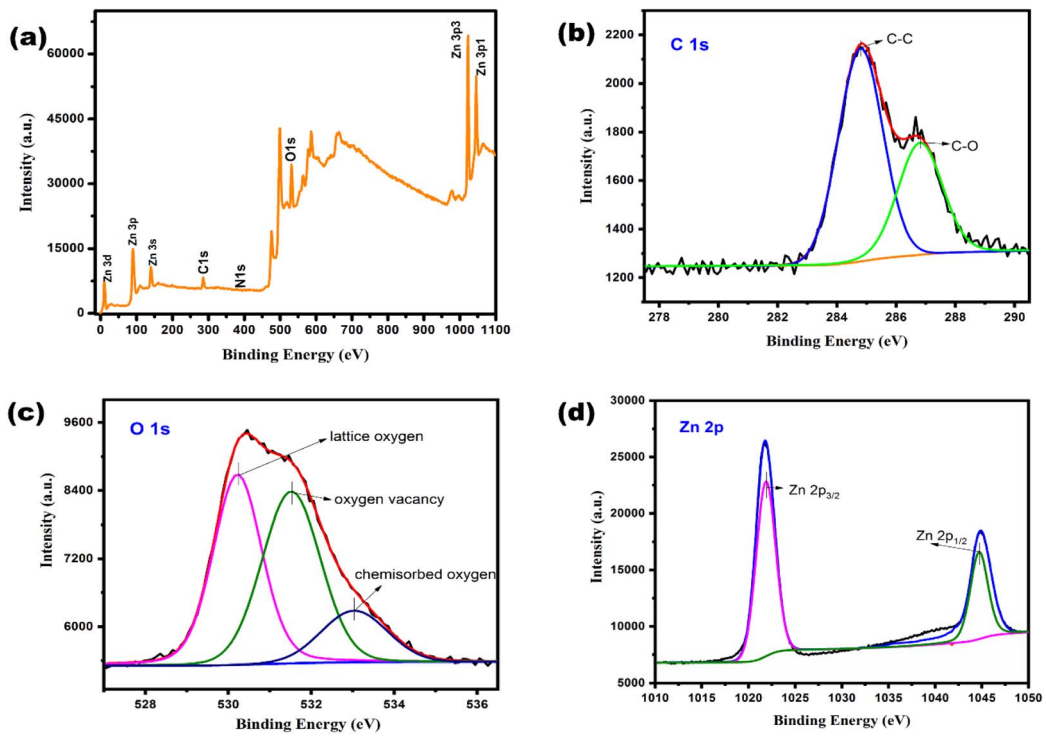

Fig. 5 XPS (a) survey spectrum, and high resolution (b) C 1s, (c) O 1s, and (d) Zn 2p spectra of Z500.

286.8 eV corresponding to the sp^2 hybridized carbon from the carbon layer (C–C) and hydroxyl carbon (C–O) respectively which indirectly evidences the existence of defects after thermal treatment.[43] No peak associated with the Zn–C bond (between 282 and 284 eV) was observed implying that carbon is mainly modified on the surfaces and sub-surfaces.[44] Similarly, the high-resolution O 1s spectrum was fitted to three peaks at 530.2 eV, 531.5 eV and 533.0 eV confirming the presence of lattice oxygen (Zn–O), oxygen vacancies on the surface of ZnO and chemisorbed oxygen, respectively.[44,45] Meanwhile, Zn 2p peaks found at 1021.8 eV and 1044.6 eV can be assigned to Zn $2p_{3/2}$ and Zn $2p_{1/2}$, inferring the existence of zinc as Zn^{2+} ions. Similar results were observed for both Z300 and Z750 (Fig. S7 and S8†). From these XPS spectra, we found that, as the calcination temperature increases from 300 °C to 500 and 750 °C, more defects are created on the sample surface and these defects may contribute to better catalytic efficiency of Z500 and Z750 towards ammonium perchlorate thermal decomposition.

TG and DSC analyses

Using thermogravimetric and differential scanning calorimetric techniques, the catalytic efficacy of the synthesized samples in AP thermal decomposition was studied in detail. The TG and DTG results are shown in Fig. 6 and S9.† Based on the TG results, AP thermolysis proceeds through a distinguishable two-stage decomposition, one at a lower temperature – LTD (below 300 °C), and the other at a higher temperature – HTD (above 300 °C), which are responsible for almost '30% and complete' decomposition of AP respectively. In this study, AP decomposition started around 270 °C and ended around 350 °C. Previous studies reveal that the introduction of additives has a significant impact on how quickly AP decomposes. Drastic changes observed in the decomposition pattern of AP after the addition of the synthesized ZnO samples (Fig. 6) authenticate the aforementioned statement. The DTG curves also show that in the presence of the synthesized samples, AP follows a multiple-stage breakdown pattern that begins early and terminates early with a tendency to merge. Although Z300 exhibits more characteristics of ZIF-8 than ZnO, it nevertheless efficiently catalyzes AP decomposition. Compared to Z500 and Z750, the less catalytic activity of Z300 is because of the presence of the 2-methylimidazole ligand in Z300. The 2-methylimidazole entity has good thermal stability due to the presence of strong H-bonding interactions *via* methyl 'H' atoms and ring 'N' atoms present in it.[46] Among the samples Z500 and Z750, Z500 was found to be a superior catalyst to Z750, as it exhibits outstanding catalytic performance in AP pyrolysis by reducing decomposition temperature to a lower value. In addition, the decomposition thermogram of AP is found to be smoother in the presence of Z500 than pure AP, AP + Z300, and AP + 750 and also tends to merge. This significant shift in decomposition temperature along with the inclination to follow a single-stage decomposition pattern in the presence of additives attests to the excellent catalytic efficiency of the synthesized ZnO samples. This amalgamation behaviour of AP when Z500 is present further supports the excellent catalytic efficacy of Z500. Phenomenological information on AP thermal decomposition with and without ZnO is given in Table 2.

Table 2 Phenomenological data of TG-DTG analysis of AP with and without catalysts

	LTD (°C)			HTD (°C)		
Samples	Ti	Ts	Tf	Ti	Ts	Tf
AP	256	270	296	296	338	347
AP + Z300	256	277	296	296	314	323
AP + Z500	246	256	259	259	266	289
AP + Z750	249	258	267	267	274	292

To further explore the exothermicity and endothermicity involved in the ammonium perchlorate thermolysis, DSC analysis was used (Fig. 7). Fig. 7 depicts the three stages of AP pyrolysis, which include an endothermic process at about 242 °C corresponding to the transition from the orthorhombic to the cubic phase and two exothermic stages that are indicative of the LTD and HTD processes.

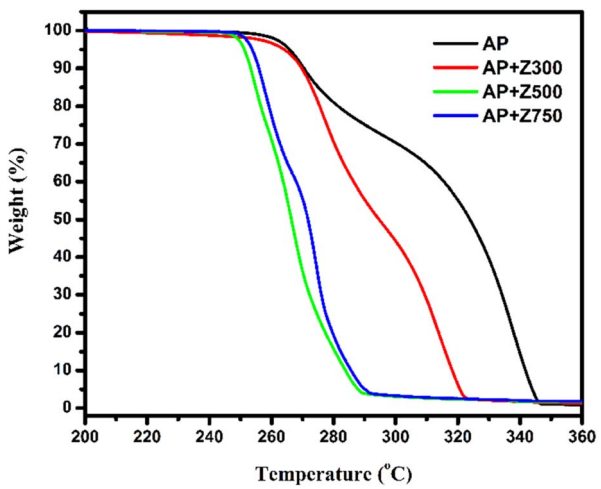

Fig. 6 TGA curves of AP, AP + Z300, AP + Z500, and AP + Z750.

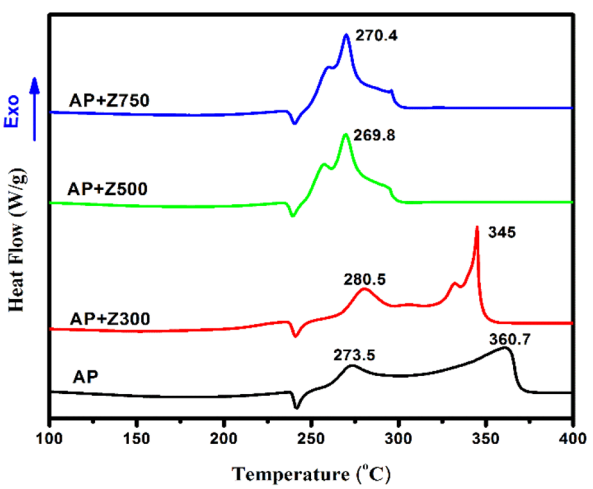

Fig. 7 DSC curves of AP, AP + Z300, AP + Z500, and AP + Z750.

The weak exothermic peak at 273 °C (LTD) implies the partial decomposition of AP with the formation of some intermediate products followed by an HTD peak at around 361 °C. This intense exothermic peak is indicative of the complete breakdown of the remaining AP and intermediated products formed earlier.[47] In the presence of Z500 and Z750 a radical change is observed in the AP decomposition pattern. As already noted, these samples effectively catalyze the translation of a two-stage process into a single-stage process with a marked reduction in decomposition temperature. And this behaviour effectually satisfies the requirements for a top-notch catalyst for solid propellants. Therefore, out of the three, Z500 is the better catalyst because (i) it has the lowest decomposition temperature, (ii) more mesoporosity than Z750, and (iii) more polar (0001) facets than Z750, which facilitate the faster decomposition of AP.

Another crucial metric to indicate the pyrolysis behaviour of AP is the activation energy. By conducting a thorough kinetic analysis using the KAS method (eqn (1)), the catalytic performance of the sample Z500 towards AP breakdown was further investigated. For this, the samples (AP and AP + Z500) were heated at 5 heating rates 2, 3.5, 4, 5, and 7.5 °C min^{-1}. The activation energies (E_a) for AP and AP with Z500 were calculated using the given equation at various degrees of conversion (α), from 10 to 90% weight loss.

$$\ln\left[\frac{\beta}{T_\alpha^2}\right] = \ln\left[\frac{AR}{E_a}\right] - \frac{E_a}{RT_\alpha} \quad (1)$$

where β is the heating rate in °C min^{-1}, A is the pre-exponential factor, R is the universal gas constant, and T_α is the temperature at a fixed degree of conversion. From the above equation, the plot of $\ln[\beta/T_\alpha^2]$ *vs.* $1/T_\alpha$ would result in a straight line with a slope of $-E_a/R$, from which activation energy can be derived. From the above calculations, the activation energies for AP and AP + Z500 were found to be 149.2 kJ mol^{-1} and 130.4 kJ mol^{-1} respectively. The result indicates that Z500 has obvious catalytic efficiency towards AP thermal decomposition and this might be due to the presence of abundant (0001) planes on the surface of Z500, which is similar to previous reports.[32,47] The availability of more polar planes will facilitate the faster decomposition of ammonium perchlorate. A comparison of thermal decomposition studies of AP in the presence of MOFs[48–51] and MOF-derived metal oxides[17,18,24] is given in Table 3.

From the above table, it is clear that MOFs and MOF-derived metal oxides have recently been well explored as potential catalysts for AP thermal decomposition studies, and better results were obtained upon using higher weight percentages of catalysts. Considering the complicated and tedious synthesis routes employed, the resultant catalytic performance, and the large amount of catalyst used, ZIF-8-derived ZnO is undoubtedly superior to the above-mentioned MOF-based additives in terms of its facile synthesis, eco-friendliness and excellent catalytic efficacy with a lower amount of catalyst (1 wt%). Practically, a higher amount of catalyst will affect the oxidizer content in the system and thus have adverse impacts on its energetics. Here, in this work, we could achieve a better result compared to the previous reports by using a minimal amount of catalyst. Since the synthesis procedure is very simple, it can also be easily scalable to larger amounts.

Table 4 provides a comparison of the sustainability of MOFs reported for AP thermolysis. As per the table, a catalyst is said to be sustainable only if it follows the above-mentioned conditions. Concerning conventional synthetic systems and conditions, many efforts are being made by researchers to bring sustainability to their work by adhering to these conditions. But, the simplest yet challenging condition that no one complies with is the use of water as the solvent and the use of renewable raw materials. From the above table (Table 4), we can observe that ZIF-8 derived ZnO is an environmentally benign facile catalyst as it satisfies most of the aforementioned conditions like the use of water as the solvent, use of less hazardous reagents, facile and easily scalable synthesis route, economic viability, and energy efficiency. Therefore, in light of both catalytic performance and sustainability, ZIF-8-derived ZnO is the most potential catalyst candidate.

TG-MS analysis

Though the thermal decomposition and kinetic parameters for AP pyrolysis have already been studied extensively, the detailed mechanism of thermal decomposition remains uncertain. Hyphenated techniques (like TG-MS) are proven to be efficient in elucidating such mechanisms. These techniques permit the

Table 3 Comparison of the catalytic performances of reported MOFs for AP thermolysis

Catalyst used	Synthesis method employed	Specific surface area (m^2 g^{-1})	Amount of catalyst used (wt%)	ΔHTD (°C)	Ref.
HKUST-1 derived CuO	Mechanochemical air flow synthesis of HKUST-1 followed by calcination	8.05	10	86	17
Cu-MOF derived Cu/Cu_2O/C	Hydrothermal synthesis followed by calcination	76.6	10	87.5	18
ZIF-67 derived Co_3O_4@C	High-temperature calcination in an argon atmosphere	210	10	91.5	21
Fe-BTC	Commercially available	—	1	10	48
$[Ag(tntrza)]_n$	Reaction between $AgNO_3$ and tntrza	—	10	85	49
$Cu_2(bdc)_2(bpy)$-MOF	Hydrothermal approach	473	2	61	50
Zn-MOF	Simple mixing with heating followed by calcination	—	5	50	51
ZIF-8 derived ZnO	Calcination (air)	9.4	1	90	This work

Table 4 Sustainability comparison of reported MOFs for AP thermolysis[a]

	Sustainability conditions							
Catalyst used	Minimal waste generation	Use of renewable raw materials	Energy efficiency	Non-toxic or less toxic	Use of water as solvent	Easy separation & purification	Long-term economic viability	Ref.
HKUST-1 derived CuO	✓	✗	✓	✓	□	✓	✓	17
Cu-MOF derived $Cu/Cu_2O/C$	✓	✗	✓	✓	✓	✓	✓	18
ZIF-67 derived Co_3O_4@C	✓	✗	✗	✓	✗	✓	✗	21
Fe-BTC	✓	✗	✓	✓	□	✓	✓	48
$[Ag(tntrza)]_n$	✗	✗	✗	✗	✗	✗	✗	49
$Cu_2(bdc)_2(bpy)$-MOF	✗	✗	✓	✗	✗	✓	✗	50
Zn-MOF	✓	✗	✓	✓	⊠	✓	✓	51
ZIF-8 derived ZnO	✓	✗	✓	✓	✓	✓	✓	This work

[a] ✓ – follows the condition, ✗ – doesn't follow the condition, □ – solvent free, and ⊠ – use of water and DMF as solvents.

real-time evaluation of evolved gases during thermal decomposition, which allows the determination of the chemical decomposition mechanism.[52] In this study, the decomposition fragments of AP were found to be at m/z values 16, 30, 32, 35, 36, 44, 46, and 70, which can be likely assigned to NH_2^+/O^+, NO^+, O_2^+, Cl^+, HCl^+, N_2O^+, NO_2^+, and Cl_2^+, respectively. Apart from these products, isotopes of chlorine were also identified at m/z values 37 $(^{37}Cl)^+$, 38 $(H\,^{37}Cl)^+$, 72 $(^{35}Cl\,^{37}Cl)^+$, and 74 $(^{37}Cl_2)^+$. The results of TG-MS analysis are shown in Fig. S10a and b,† depicting a clear association of TG findings with MS curves. Like TG and DSC results, the TG-MS curves of AP also follow a two-stage decomposition pattern, which corresponds to LTD and HTD stages. Uncatalyzed AP decomposition starts around 260 °C with the evolution of N_2O as the major product. With a short period of stagnation, the HTD phase starts with the evolution of more gaseous products such as Cl, HCl, NO, NO_2 and Cl_2. According to Fig. S10a,† the higher concentration of N_2O (m/z = 44) at lower temperatures approves the notion that NH_3 first oxidizes to form N_2O.[53] This is due to the lack of active oxygen in the system during the LTD stage, which inhibits the oxidation of N to a higher valence state.[21,23] In the presence of Z300, the decomposition pattern of AP does not show any drastic changes. Instead, it still follows a double-stage decomposition pathway with a small shift in onset temperature to a lower value. Different from this, under the action of catalysts Z500 and Z750, the AP onset decomposition temperature has shifted to a much lower value implying the good catalytic efficacy of the synthesized catalysts towards AP decomposition. Unlike two distinct stages of AP decomposition, Z500 and Z750-led AP decomposition exhibit two consecutive characteristic decomposition peaks, which have a high tendency to get merged. Also, under the action of synthesized ZnO, the decomposition behaviour of AP occurs in advance implying the quicker decomposition of $HClO_4$ leaving a higher concentration of active oxygen in the system.[21] This subsequently will lead to the faster oxidation of NH_3 to oxides of N. According to the literature, more evolution of NO_2 was observed at the HTD stage as complete oxidation of ammonia occurs at higher temperatures. Here, the NO_2 evolution pattern seems different in the presence of catalysts. Under the action of catalysts, more NO_2 evolution is observed at low temperatures instead of high temperatures. This might be because, more ammonia is getting oxidized at lower temperatures in the presence of the catalysts, which might be due to the augmented decomposition of AP.

Mechanism

A plausible mechanism for the outstanding catalytic activity of the synthesized ZIF-8-derived ZnO samples (Fig. 8) can be as follows. As mentioned above, the pyrolysis of AP involves two stages: LTD and HTD. The low-temperature decomposition is a heterogeneous process that proceeds *via* proton transfer from ammonium ions to perchlorate ions to form ammonia and perchloric acid. These intermediate products NH_3 (g) and $HClO_4$ (g) then get adsorbed to the surface of un-decomposed AP.[47] As widely known, AP decomposes only partially at low temperatures. According to Boldyrev, it is assumed that for the reaction to continue in the adsorbed layer, perchloric acid is desorbed more quickly than ammonia; this leads to incomplete oxidation of ammonia and saturation of the AP surface with ammonia, which causes the reaction to stop and the incomplete transformation of perchlorate.[54] As the temperature rises, the HTD stage is proposed to involve (i) the desorption of adsorbed molecules, (ii) an oxidation–reduction reaction between NH_3 (g) and $HClO_4$ (g) to form low molecular weight products and (iii) the dissociation of un-decomposed AP.[47] In the presence of an additive, this process becomes faster, causing the quicker decomposition of AP.

For ZnO, large exposed (0001) facets present will promote the faster adsorption of perchloric acid.[32] Also, when ZnO is heated at higher temperatures, due to the low band gap of synthesized ZnO, free electrons will be generated on the ZnO conduction band.[32,55] The adsorbed perchloric acid will serve as an electron acceptor for these electrons to form superoxide radical anions (O_2^-). These superoxide anions that are excellent oxidizing

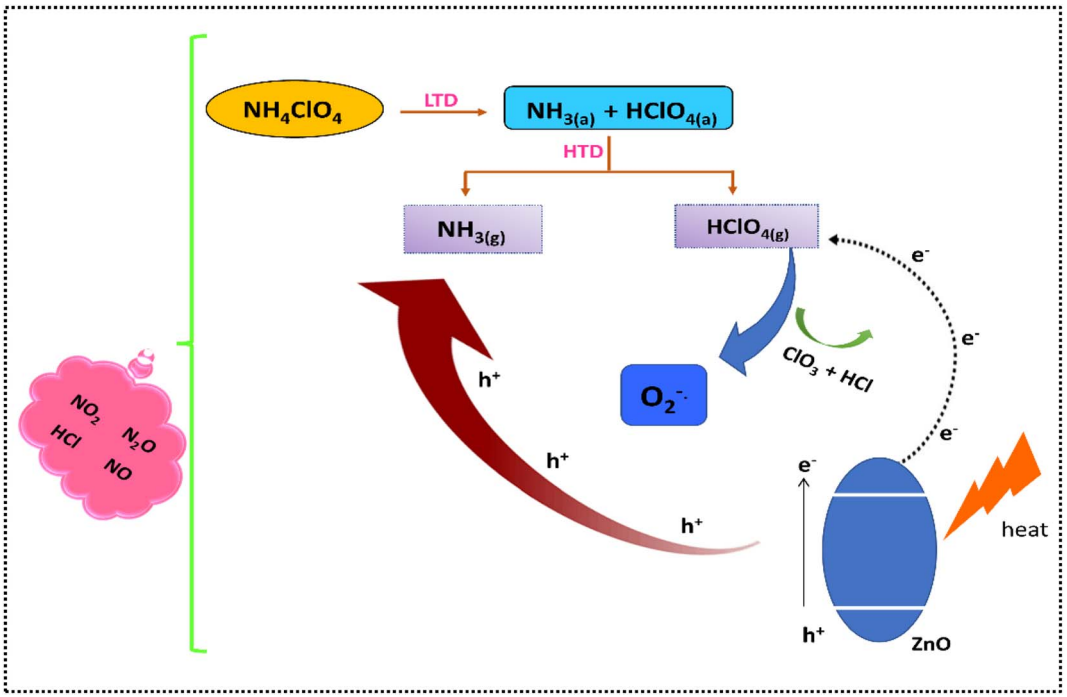

Fig. 8 The plausible mechanism of thermal decomposition of AP in the presence of the catalyst ZnO.

agents in nature along with the lattice oxygen present on the ZnO surface will enable the faster oxidation of NH_3 to higher oxides of N (NO_2, N_2O and NO).[4,12] Thus, faster decomposition of AP occurs in the presence of ZnO. From the TG and DSC data, it is clear that the catalytic efficacy of the synthesized samples lies in the order Z300 < Z750 < Z500. This can be accounted for by the availability of exposed (0001) sites present in the synthesized ZnO. Hence, ZnO with relatively more (0001) facets – Z500 – was found to be the better catalyst, which facilitates the easy and faster adsorption of perchloric acid onto the ZnO surface during the decomposition reaction. This will subsequently avoid the accumulation of $HClO_4$ and ammonia on the ammonium perchlorate surface, facilitating a complete decomposition process.

Conclusions

In summary, ZIF-8-derived ZnO was synthesized *via* a simple calcination method at different temperatures. In contrast to the expensive and laborious synthesis of other MOFs requiring hazardous reagents and toxic chemicals, ZIF-8 synthesis is a quick and sustainable process requiring minimal reagents and water as the medium. The calcination of ZIF-8 at 300 °C was insufficient for the formation of ZnO while annealing at 500 °C and 750 °C yields crystalline wurtzite ZnO. The synthesized catalysts are facile, easy to prepare, low-cost, eco-friendly, and sustainable. Morphology studies reveal that synthesized Z500 is in the nanometer regime with an average particle size of 52 nm. The XPS study shows that zinc is in a Zn^{2+} oxidation state with the presence of surface-modified carbon. UV-vis DRS spectra validate the tunability of the synthesized zinc oxides with calcination temperature, and the narrowing of band gaps will result in the availability of more charge carriers for the reaction, which will enhance the oxidation–reduction reactions of perchloric acid and ammonia formed during the decomposition of AP. This claim was well substantiated by thermal analyses. In the presence of 1 wt% Z500, AP thermal decomposition temperature was decreased by 90 °C and the activation energy was reduced from 149 kJ mol^{-1} to 130 kJ mol^{-1}. Hence, the ZIF-8 derived catalyst, Z500, is an eco-friendly, facile, and economical catalyst for ammonium perchlorate thermal decomposition, which can proficiently cater to the quest for eco-friendly facile catalysts for propellants with reduced mass penalties.

Conflicts of interest

The authors declare no conflicts of interest.

Acknowledgements

GM is grateful to the University Grant Commission (MANF), India and AVK is grateful to Mahatma Gandhi University, Kottayam for the financial assistance. The authors are also thankful to CLIF – Trivandrum, VSSC – Trivandrum, NIIST – Trivandrum, and MGU-Kottayam for providing all the analytical facilities. We are also indebted to Dr P. Radhakrishnan Nair, Dr Marilyn Mary Xavier, Bhagyalakshmi Balan and Sreerenjini C R for all the fruitful discussions.

References

1 L. Tian, J. X. He, X. Y. Huang, Y. Feng, Y. W. Lu, R. H. Wang, Q. Wang and C. P. Guo, *React. Kinet., Mech. Catal.*, 2023, 1–10.

2 Y. Lu, J. He, W. Tong, J. Hou, J. Han and L. Yang, *J. Anal. Appl. Pyrolysis*, 2022, **163**, 105495–105504.
3 J. Liu, H. Yu, L. Wang, S. Z. Vatsadze, Z. Huang and B. U. Amin, *J. Organomet. Chem.*, 2022, 122514–122521.
4 P. Zhou, S. Zhang, Z. Ren, Y. Wang, Y. Zhang and C. Huang, *Inorg. Chem. Front.*, 2022, **9**, 5195–5209.
5 C. Zhang, X. Yang, Z. Zhang, J. Li, W. Jin and H. Ma, *Surf. Interfaces*, 2022, **35**, 102425–102435.
6 D. Liu, C. Xuan, L. Xiao, Y. Hu, G. Zhang, F. Zhao, H. Gao, W. Jiang and G. Hao, *Langmuir*, 2022, **38**, 15234–15244.
7 T. Wen, Y. Feng, Y. Bi, L. Xu and C. Guo, *Mater. Today Commun.*, 2022, **33**, 104294–104300.
8 G. Mani, P. R. Nair and S. Mathew, *ACS Omega*, 2022, **7**, 38512–38524.
9 G. Zhang, X. Yu, Z. Wang, S. Li, Y. Zhu, Y. Wang and X. Xiao, *J. Alloys Compd.*, 2023, **942**, 169075–169085.
10 B. Ye, K. Li, C. Feng, C. An, J. Wang and Y. Zhang, *Vacuum*, 2023, **207**, 111509.
11 S. Wang, B. Ye, C. An, X. Song and J. Wang, *J. Mater. Sci.*, 2020, **55**, 4646–4655.
12 X. Bu, F. Liu, Z. Zhang, Z. Wang, J. Liu and W. Liu, *Mater. Lett.*, 2018, **219**, 33–36.
13 Y. Liu, H. Liu, B. Huang, T. Li and J. Wang, *CrystEngComm*, 2017, **19**, 5774–5779.
14 S. Tian, N. Li, D. Zeng, H. Li, G. Tang, A. Pang, C. Xie and X. Zhao, *CrystEngComm*, 2015, **17**, 8689–8696.
15 N. M. Juibari and S. Tarighi, *J. Alloys Compd.*, 2020, **832**, 154837.
16 L. L. Zulfa, R. Ediati, A. R. P. Hidayat, R. Subagyo, N. Faaizatunnisa, Y. Kusumawati, D. Hartanto, N. Widiastuti, W. P. Utomo and M. Santoso, *RSC Adv.*, 2023, **13**, 3818–3834.
17 Z. Guo, Q. Zhang, H. Liu, H. Zhang, J. Zhang, J. Zuo, B. Jin and R. Peng, *Mater. Today Commun.*, 2021, **26**, 102139–102146.
18 J. Yan, H. Wang, B. Jin, M. Zeng and R. Peng, *J. Solid State Chem.*, 2021, **297**, 122060–122069.
19 Y. Zhang, Z. Li, F. Gao, Z. Ma, W. Li, X. Gao and G. Fan, *J. Solid State Chem.*, 2022, **316**, 123551–123558.
20 M. Y. Zorainy, S. Kaliaguine, M. Gobara, S. Elbasuney and D. C. Boffito, *J. Inorg. Organomet. Polym. Mater.*, 2022, **32**, 2538–2556.
21 P. Zhou, S. Zhang, Z. Ren, X. Tang, K. Zhang, R. Zhou, D. Wu, J. Liao, Y. Zhang and C. Huang, *Adv. Sci.*, 2022, **9**, 2204109.
22 P. Zhou, X. Tang, Z. Ren, Z. Zheng, K. Zhang, R. Zhou, D. Wu, J. Liao, Y. Zhang and C. Huang, *Small*, 2023, **19**, 2207023.
23 P. Zhou, Z. Ren, X. Tang, Z. Zheng, K. Zhang, J. Liao, Y. Zhong, Y. Zhang and C. Huang, *Adv. Funct. Mater.*, 2023, 2300661.
24 H. Liu, Z. Guo, Q. Zhang, B. Jin and R. Peng, *ACS Omega*, 2021, **6**, 25440–25446.
25 X. Han, L. Zhou, S. Cao, L. Zhang, G. Xiang and J.-F. Chen, *Energy Fuels*, 2021, **35**, 4447–4456.
26 Y. Zhang, B. Lin, J. Wang, J. Tian, Y. Sun, X. Zhang and H. Yang, *J. Mater. Chem. A*, 2016, **4**, 10282–10293.
27 J. Lin, L. Huang, H. Ou, A. Chen, R. Xiang and Z. Liu, *RSC Adv.*, 2021, **11**, 21414–21425.
28 J. Lv, C. Zhang, S. Wang, M. Li and W. Guo, *Analyst*, 2021, **146**, 605–611.
29 G. Tang, Y. Wen, A. Pang, D. Zeng, Y. Zhang, S. Tian, B. Shan and C. Xie, *CrystEngComm*, 2014, **16**, 570–574.
30 S. Cho, J. W. Jang, J. S. Lee and K. H. Lee, *Langmuir*, 2010, **26**, 14255–14262.
31 H. Li, K. Zhao, S. Tian, D. Zeng, A. Pang, X. Wang and C. Xie, *RSC Adv.*, 2017, **7**, 40262–40269.
32 G. Tang, S. Tian, Z. Zhou, Y. Wen, A. Pang, Y. Zhang, D. Zeng, H. Li, B. Shan and C. Xie, *J. Phys. Chem. C*, 2014, **118**, 11833–11841.
33 G. Li, T. Hu, G. Pan, T. Yan, X. Gao and H. Zhu, *J. Phys. Chem. C*, 2008, **112**, 11859–11864.
34 J. Wang, X. Luo, C. Young, J. Kim, Y. V. Kaneti, J. You, Y.-M. Kang, Y. Yamauchi and K. C. W. Wu, *Chem. Mater.*, 2018, **30**, 4401–4408.
35 Z. Zhang, X. Luo, B. Wang and J. Zhang, *ACS Appl. Energy Mater.*, 2019, **2**, 2760–2768.
36 J. B. James and Y. Lin, *J. Phys. Chem. C*, 2016, **120**, 14015–14026.
37 K. Devarayapalli, S. P. Vattikuti, K. S. Yoo, P. Nagajyothi and J. Shim, *J. Electroanal. Chem.*, 2020, **878**, 114634.
38 Y. Du, R. Chen, J. Yao and H. Wang, *J. Alloys Compd.*, 2013, **551**, 125–130.
39 P. Norouzzadeh, K. Mabhouti, M. Golzan and R. Naderali, *Appl. Phys. A*, 2020, **126**, 1–13.
40 H. Zhang, Y. Wang, W. Zhao, M. Zou, Y. Chen, L. Yang, L. Xu, H. Wu and A. Cao, *ACS Appl. Mater. Interfaces*, 2017, **9**, 37813–37822.
41 M. Ikram, H. Lv, Z. Liu, K. Shi and Y. Gao, *J. Mater. Chem. A*, 2021, **9**, 14722–14730.
42 X. Liu, J. Zhang, Y. Dong, H. Li, Y. Xia and H. Wang, *New J. Chem.*, 2018, **42**, 12180–12187.
43 X. Liang, X. Xu, Z. Man, B. Quan, B. Sun, J. Chen, W. Gu and G. Ji, *Inorg. Chem. Front.*, 2019, **6**, 2521–2527.
44 S. Liu, J. Wang and J. Yu, *RSC Adv.*, 2016, **6**, 59998–60006.
45 L. Zhang, Q. Liang, P. Yang, Y. Huang, Y. Liu, H. Yang and J. Yan, *New J. Chem.*, 2019, **43**, 2990–2999.
46 M. Waser, *Asymmetric Organocatalysis in Natural Product Syntheses*, Springer, London, 2012.
47 H. Chai, G. Li, X. Xiang and X. Hu, *Chem. Phys. Lett.*, 2019, **730**, 460–465.
48 Y. Yang, Y. Bai, F. Zhao, E. Yao, J. Yi, C. Xuan and S. Chen, *RSC Adv.*, 2016, **6**, 67308–67314.
49 F. Yang, Y. Xu, P. Wang, Q. Lin and M. Lu, *ACS Appl. Mater. Interfaces*, 2021, **13**, 21516–21526.
50 S. Lashgari, M. S. Baei, F. F. Abkanar and S. Ghasemi, *J. Solid State Chem.*, 2021, **295**, 121940.
51 B. J. Tan, J. T. Ren, B. H. Duan, M. H. Xu, S. L. Chen, H. Zhang and N. Liu, *Dalton Trans.*, 2022, **51**, 7804–7810.
52 A. Benhammada and D. Trache, *Appl. Spectrosc. Rev.*, 2020, **55**, 724–777.
53 W. Zhang, P. Li, H. Xu, R. Sun, P. Qing and Y. Zhang, *J. Hazard. Mater.*, 2014, **268**, 273–280.
54 V. Boldyrev, *Thermochim. Acta*, 2006, **443**, 1–36.
55 P. Mitra, A. P. Chatterjee and H. S. Maiti, *Mater. Lett.*, 1998, **35**, 33–38.